

Cladding pressures and primary structural system forces of a wood building exposed to strong winds

Ioannis Zisis¹, Ted Stathopoulos², Ian Smith³ and Ghasan Doudak⁴

¹Graduate Research Assistant, Building Aerodynamics Laboratory, Centre for Building Studies, Concordia University, Montreal, QC, Canada, H3H 2W1, i_zisis@live.concordia.ca

²Professor and Associate Dean, Building Aerodynamics Laboratory, Centre for Building Studies, Concordia University, Montreal, QC, Canada, H3H 2W1, statho@bcee.concordia.ca

³Professor, Forestry & Environmental Management, University of New Brunswick, Fredericton, NB, Canada, E3B 5A3, ismith@unb.ca

⁴Manager, Wood and Structural Standards, Canadian Wood Council, Ottawa, ON, Canada, K1P 6B9, gdoudak@cwcc.ca

Abstract

Several studies have been carried out on the evaluation of wind-induced pressures on building envelopes. However, there is very limited research on wind-induced forces on the main structural elements of a building including its foundation. Thus, a full-scale monitoring research project was initiated to examine the wind-induced structural forces of a low-rise wood building. The field facilities include two weather stations and a test house equipped with load and pressure sensors. The house is resting on top of twenty-seven load cells and is structurally isolated i.e. the only points of contact between the foundation wall and the superstructure are the load cells. Simultaneously to the load monitoring, forty pressure taps are recording the envelope pressures both at the roof and the wall surfaces. In addition to the field monitoring, a scaled model of the house was tested in a boundary layer wind tunnel using three different upstream terrain configurations, to simulate winds coming from different directions.

The analysis of the wind speed and direction field data confirmed the non-uniform variation of the basic terrain properties over the wind direction and this was also verified in the comparison of the field with the wind tunnel results. These comparisons were made in the form of both envelope pressures and total uplift forces at the foundation level and provided useful insight regarding the wind load path inside the structural elements of the building. Experimental findings were also compared to the Canadian Code and American Standard wind provisions indicating that there is a clear underestimation of the total uplift force when this is estimated on a code/standard basis, in its current state.

Keywords

Full-scale monitoring, wind tunnel experiments, low-rise wood building, envelope pressures, wind uplift forces.

1. Introduction

The majority of dwellings in North America are light-weight, low-rise structures of simple geometry and layout. Wind-induced loading is of major importance during the design of these structures and wind-related standards have been developed and revised numerous times, resulting into a more complex yet safer and more economical design process. However, recent extreme wind events and growth of wind-related losses indicate that this process still needs further refinement and attention.

Wind effects on low buildings have been examined extensively the past few decades. The availability of boundary layer wind tunnels had also significant influence to the current wind standards (Davenport et al. 1977 and 1978). In addition, several full-scale studies were carried out and contributed to the verification of the results from simulation studies. Almost all of these studies have been focusing extensively on how the pressure distribution can be precisely and accurately predicted (Eaton and Mayne 1975, Robertson and Glass 1988, Ng and Mehta 1990, Levitan et al. 1990). In addition, technological advancement and increase of computing power have introduced new computational tools into the experimental wind engineering approach. The link between the pressure prediction and the actual wind-induced structural response stage was traditionally weak and often transferred to other disciplines (structural engineers and finite element modelling experts). This needs to be carefully addressed and the current study is aiming exactly at the interconnection of the two disciplines i.e. wind and structural engineering.

The potential of wind-structure interaction through full-scale studies was acknowledged and proposed by researchers as the most reliable tool to validate wind tunnel experiments (e.g.

Davenport 1975 and 2002). Lack of significant field studies related to wind load paths, initiated the present collaborative effort, which has as main objective to better understand and define how wind pressure is transformed into a set of forces transferred through building elements to the foundation level. In addition to the envelope pressure characteristics, force data will provide the appropriate information to successfully map the wind load flow. Each of the structural components has its own importance and effect in the total response and reaction of the structure. Dissipation of the applied energy occurs at various stages and in most cases is part of a highly non-linear process. In some cases these phenomena are treated from current provisions by approximations; e.g. the 30% reduction of the effective wind load for the design of the foundation, suggested by National Building Code of Canada (NBCC 2005, Users Guide - Figure I-7). The need for a facility capable of capturing real wind events in the form of, not-only wind-induced pressures on the building envelope, but also in resulting structural forces is clear.

2. Project description

2.1 Full-scale facilities

The full-scale facilities include an experimental single-storey wood building and two meteorological towers. The experimental house is located in Fredericton (NB) and it was built for the particular needs of this research project (Doudak 2005, Zisis and Stathopoulos 2009). The building has a rectangular layout with external dimensions of 8.6 x 17.2 x 5.6 meters (W x L x H), a duo-pitch roof of 4/12 slope and rests on a concrete foundation wall 0.225 m thick and 1.225 meters deep. The geometry and dimensions of the house are shown in Fig. 1. The orientation of the building is 43 degrees right of the geometric North which was assumed to be the reference zero point for all wind direction measurements. Four

anemometers are monitoring the wind speed and direction. Three of them are mounted on a 10-meter mast on the North-West side of the house at 5.5, 6.5 and 10.0 meters height and the fourth is mounted on the top of a 5.5-meter post on the South-East side of the house.

The load cell system is an innovative part of this study. A total number of twenty-seven 3-D load cells were placed around the perimeter of the building at the foundation-to-wall interface. Another six 1-D load cells were also installed between the wall top plate and three of the roof trusses but the results obtained from those have not been considered in this paper. It should be mentioned that the building is completely isolated from the foundation and the only points of contact are the 3-D load cells. This construction detail assures the transfer of any applied load to the foundation only through the load cells. Furthermore, the monitoring of the wind-induced envelope pressures was achieved through the forty pressure taps, twelve of which located on the wall and twenty-eight on the roof. The location of the load cells and pressure taps is shown in Fig. 2. The temperature was also monitored using thermocouples installed at various locations.

2.2 Wind tunnel tests

A model of the test house and its surroundings was constructed and tested in the boundary layer wind tunnel of the Building Aerodynamics Laboratory at Concordia University. The model is of geometric scale of 1:200 and is equipped with 126 pressure taps located on the wall and roof surface (Fig. 3). Forty of these taps correspond to their appropriate full-scale location (see Fig. 2). All wind tunnel tests were conducted for thirty-six wind angles of attack in 10° increments. The wind velocity and turbulence intensity profiles were measured using the 4-hole Cobra probe (TFI) and sampling rate of 1000 Hz. The gradient wind velocity for all tests was 13.5 m/s. Three different upstream terrain configurations were considered for the wind tunnel tests representing open, light suburban and heavy suburban exposures. The

power law coefficients for these tests were 0.16, 0.22 and 0.28 (see Fig. 4) whereas the turbulence intensity levels at the ridge height were 17.9, 20.2 and 26.4% respectively. The pressure measurements on the model were conducted using a system of miniature pressure scanners from Scanivalve (ZOC33/64Px) and the digital service module DSM 3400.

3. Experimental results

3.1 Weather tower - Exposure effects

The experimental house is located in a relatively open-suburban area with some low-height obstacles in the proximity. In order to verify the above subjective observation, the basic exposure characteristics (power law exponent, turbulence intensity and roughness length) were evaluated using field data acquired from the two anemometers of the North-West meteorological tower (at 6.5 and 10.0 meters height). Records collected during October to November 2008 and April to June 2009 were considered for this analysis and power law exponent, turbulence intensity and roughness length values were calculated with respect to the approaching wind direction. The results are based on 10-minute averaged statistical values (mean and standard deviation) and were filtered to retain data with mean wind speeds over 10 km/h (at 6.5-meter height) assuming stationarity is satisfied. More specifically, thirty seven individual records fulfilled the above condition, considering also that the period between December 2008 and March 2009 the data acquisition system was not operational due to lower temperatures and snow accumulation on top of the roof.

The results were plotted in terms of power law exponent, turbulence intensity and roughness length for all available full-scale wind directions and presented in Figs. 5, 6 and 7 respectively. The power law exponent ranges from 0.05 to 0.50, the turbulence intensity from 20% to 50% and the roughness length from a few millimeters up to 1.2 meters. Even if the

data are grouped within a wind direction range that results into similar properties (e.g. South-West region) the mean values still vary significantly. For instance, the power law exponent takes its highest mean value of 0.36 (0.08 standard deviation) for the wind direction range 230°-290°, whereas the lowest mean value of 0.20 (0.05 standard deviation) occurs at the 70°-125° range. However, this approach results into more consistent turbulence intensity values (32% to 37%) for all wind direction ranges.

It is quite interesting to examine how these properties vary for different angles of attack, considering that the test house, as previously indicated, is located in a relatively open area with only few low-rise buildings and medium height trees in the proximity. Following current wind provision guidelines and “common” wind engineering sense, the terrain would be classified in the open to suburban region expecting a power law exponent in the range of 0.20. The higher variations should be clearly attributed to the influence of adjacent buildings (north and south sides) and forestry area (east side) located inside a radius of 300-400 meter fetch. These deviating terrain properties indicate that complex terrains need to be examined carefully in order to properly conduct scaled model tests and compare full-scale to wind tunnel results successfully.

3.2 Pressure coefficient comparisons

To verify the agreement between the field and model scale pressure results, two field records (May 14th and June 1st, 2009) were compared to the three available wind tunnel tests (open, light suburban and heavy suburban). The full-scale records were selected based on the high wind speeds occurred for an extended duration during the 24-hour period. For this comparison two pressure taps were considered, one on the wall (Fig. 8) and one on the roof surface (Fig. 9). The mean and peak pressure coefficients were evaluated using the following equations and plotted with respect to wind direction:

$$[1] \quad c_{p,\text{mean}} = \frac{p_{\text{mean}} - p_a}{1/2\rho\overline{V_{5.5\text{m}}}^2}$$

$$[2] \quad c_{p,\text{peak}} = \frac{p_{\text{peak}} - p_a}{1/2\rho\overline{V_{5.5\text{m}}}^2}$$

where ρ =air density (kg/m^3); $\overline{V_{5.5\text{m}}}$: mean wind speed at 5.5 meters (m/s); p_a =ambient atmospheric pressure (Pa), p_{mean} =mean surface pressure (Pa) and p_{peak} =peak surface pressure (Pa). It should be noted that for the full-scale calculations the mean values were based on a 10-minute average and the instantaneous peak on a 3-second average (full-scale time scale). Moreover field data were integrated over a wind angle of attack of 10-degree range to account for the higher standard deviation values and to be directly compared to wind tunnel tests carried out using intervals of 10 degrees. To better represent the varying characteristics of the full-scale results the minimum and maximum integrated values of each set of data were considered and plotted in addition to the mean values. This range obtained by considering the mode of the extreme (minimum/maximum) probability density function assuming a Type I distribution (Gumbel).

The agreement for both mean and peak pressure coefficients is considered satisfactory. Wind tunnel values are in most cases within the range of the field results. Regarding peak pressure coefficients, the heavy suburban terrain configuration values show smaller discrepancies, particularly for those directions where the terrain properties vary the most (240° to 300° – see Figs. 5, 6 and 7).

In addition to the individual pressure tap comparisons, the wind tunnel tests are verified by comparing mean and peak pressure coefficients including this time results from all wall and roof pressure taps. In more detail, data from two wind tunnel tests (light suburban and heavy suburban) are compared to the two field records in the form of 45° scatter plots. The open terrain case was disregarded as it was assumed not to properly describe the real/field

exposure. Roof and wall pressure coefficients based on 10-minute sets from each record are presented in Fig. 10 (May 14th, 2009) and Fig. 11 (June 1st, 2009). The mean wind speed and direction for the first record was 8.36 m/s and 204°; for the second 7.06 m/s and 285°. For both cases the agreement is significantly better for the heavy suburban terrain simulation. This agreement supports the previous results and adds confidence on the verification process of the wind tunnel experimental approach.

3.3 Wall uplift participation factors

As previously discussed, an innovative part of this study is the system of twenty-seven load cells located between the concrete foundation wall and the floor I-Joist system. These load sensors capture simultaneously the wind-induced loads that flow from the superstructure down to the foundation level. Similarly to the pressure coefficient comparison, load cell data acquired during Fall 2008 (October and November) and Spring 2009 (April to June) were used to evaluate the uplift force participation of each wall during strong wind events with respect to the approaching wind angle of attack. The twenty-seven foundation load cells were grouped into four main sets, namely North-West, South-West, South-East and North East, representing the four wall segments (Fig. 12). Load readings were transformed into force coefficients ($c_{f,i}$) using the following equation:

$$[3] \quad c_{f,i} = \frac{F_i}{(1/2\rho\overline{V_{5.5m}}^2)A}$$

where ρ : air density (kg/m^3), $\overline{V_{5.5m}}$: mean wind speed at 5.5 meters (m/s), F_i : load cell force reading (N) and A : building area (m^2).

The participation of each wall to the uplift structural resistance was evaluated by considering the ratios of the instantaneous uplift force coefficient acting simultaneously on each wall segment to the instantaneous total uplift force coefficient (Fig. 13). The results

show that the dominant foundation load is transferred towards the sidewalls, as opposed to the minimal contribution from the endwalls. In more detail, the South-East wall reaches the 47% of the total uplift wind load for wind direction of 180° while it takes its minimum value of 36% as a leeward wall (270°-330 °). The North-West wall performs in a similar manner, i.e. a participation of 50% is reached when the wind is approaching from the North-West direction and a minimum of 30% is anticipated for anti-diametric wind directions. Finally, the endwalls (South-West and North-East) have significantly lower participation with their maximum ratio to the total uplift force to be up to 29% combined. If considered separately, the North-East reaches its maximum value of 26% and the South-West the value of 27.5% as windward walls.

Despite the fact that these results follow in principle what should be expected on a typical low-rise wood building with a rigid I-Joist floor system, the precise participation of each wall segment can be now incorporated on the ongoing finite element modelling of the test house which will assist to further investigate and compare simulation to field results.

3.4 Force coefficient comparisons

Full-scale data were acquired using both pressure and force sensors, whereas wind tunnel tests produced only envelope pressures. In addition to the verification of the wind tunnel simulation in the form of pressure coefficient comparisons, the total instantaneous uplift force of the building was compared to the available full-scale load data by integrating the measured envelope pressures obtained in the wind tunnel over the roof surface. Consequently, the total uplift force coefficient was calculated, and compared to that calculated directly by the load cell data, for each upstream terrain case using the following equation:

$$[4] \quad c_{f,z} = \frac{\sum c_{p,i} A_{\text{eff},i}}{A}$$

where $c_{p,i}$: instantaneous pressure coefficient, $A_{eff,i}$: effective pressure tap area (m^2) and A : building area (m^2). Similarly to the previous comparisons, for the full-scale calculations the mean force values were based on a 10-minute average and the instantaneous peak force values on a 3-second gust. The field data were filtered to retain only those for wind speeds over 8 m/sec (at 5.5 meters height). The dynamic pressure was always averaged on a 10-minute basis and was referenced to the 5.5 meters anemometer. Moreover, field data were integrated over a wind angle of attack of 10-degree range to account for the higher standard deviation values of the wind direction and to be directly compared to wind tunnel tests carried out using intervals of 10 degrees. To account for the varying characteristics of the full-scale results, the range (maximum and minimum values) of the integrated values of each set of data was considered in addition to the mean values.

The comparison of the mean total uplift force coefficients is presented in Fig. 14 and shows that all three wind tunnel upstream exposure configurations are located within the range of the field values. The discrepancies are higher for the North-West region ($230^\circ - 330^\circ$) where the mean full-scale values are up to 74% higher compared to the light suburban terrain wind tunnel test. The peak uplift force coefficient comparison is presented in Fig. 15 and shows better agreement compared to the mean values. Both positive and negative peak wind tunnel results are again within the range of the field data. The agreement is particularly improved for the heavy suburban terrain simulation, for which the full-scale minimum peak uplift force coefficients are in between the $\pm 25\%$ range compared to the wind tunnel data.

In addition to the experimental findings, the estimated total uplift force coefficients derived from the NBCC 2005 building code and ASCE 7-05 standard were also plotted in Fig. 15. For the NBCC 2005 calculations, the external peak composite pressure-gust coefficients ($C_p C_g$) from Figure I-7 were used to calculate the total uplift force coefficient. The averaging period for the reference wind pressure was adjusted from hourly to 10-minute mean. In a

similar manner, the external pressure coefficients (GC_{pf}) from Figure 6-10 (ASCE/SEI 7-05) were considered and the total uplift force coefficient was computed. For this comparison the velocity pressure was adjusted to account for the averaging period of 10 minutes instead of the 3-sec gust considered in the ASCE standard. The estimated NBCC 2005 and ASCE 7-05 values clearly underestimate the full-scale and in some cases the wind tunnel values. The ASCE 7-05 uplift force coefficient value of -1.51 is higher (absolute value) than the open and suburban terrain wind tunnel curves and for most of the directions also higher than the urban terrain. On the other hand, the NBCC 2005 value of -1.30 reflects poorly to both full-scale and urban terrain values, whereas the suburban terrain wind tunnel force coefficients exceed the estimated NBCC 2005 value for only two directions. This underestimation will become even more critical if the NBCC 2005 values are adjusted for the exposure using the factors provided in Sentence (5) of section 4.1.7.1 (NBCC 2005). For the particular building the exposure factor, which is equal to 0.90 for open terrain and 0.70 for rough terrain, would further reduce the estimated force coefficient by an additional 30% resulting into a significantly lower than the experimental findings value.

4. Conclusions

The wind-induced response of a low-rise wood building was evaluated through a unique full-scale experimental house specially built and equipped with pressure and force monitoring equipment. In addition, a scaled model of the house was tested in a boundary layer wind tunnel for three different upstream exposure configurations. The analysis of the available field and wind tunnel data showed the following:

- Data acquired from two anemometers on the North-West side of the house, indicate a non-uniform upstream exposure for different wind angles of attack, as established by power law exponents and roughness lengths.

- The comparison of the envelope pressures in form of both mean and peak pressure coefficients was satisfactory. Almost all the wind tunnel values were within the range of the full-scale values. The agreement for the peak component was particularly improved for the heavy suburban wind tunnel configuration.

- The total wind-induced foundation uplift force is mainly transferred to the two – parallel to the ridge – sidewalls. The participation factors are significantly higher, for all wind directions, for the two sidewalls compared to the North-East and South-West endwalls.

- The comparison of total uplift force coefficients between the real and model scale studies is considerably good with both mean and peak wind tunnel values located within the full-scale range. Some discrepancies exist particularly for those wind directions for which the upstream exposure is inhomogeneous.

- Finally, the estimation of the uplift force coefficient using envelope pressure values derived from NBCC 2005 and ASCE 7-05 compares poorly to the minimum peak wind tunnel and full-scale values. This underestimation is particularly critical for the NBCC 2005 if the estimated coefficient is adjusted for the exposure and foundation reduction indicated in the current version of the code.

Acknowledgements

The writers acknowledge the support received for this study from the Natural Sciences and Engineering Research Council of Canada through a cooperative research and development grant, as well as the research discovery grant to the second author. In addition, support from the Canadian Wood Council and FPInnovations is greatly appreciated.

References

- ASCE/SEI 7-05 2005. Minimum Design Loads for Building and Other Structures, American Society of Civil Engineers, New York, N.Y.
- Davenport, A.G. 1975. Perspectives on the full-scale measurement of wind effects. *Journal of Wind Engineering and Industrial Aerodynamics*, **1**, 23-54.
- Davenport, A.G. 2002. Past, present and future of wind engineering. *Journal of Wind Engineering and Industrial Aerodynamics*, **90**(12-15), 1371-1380.
- Davenport, A.G., Surry, D. and Stathopoulos, T. 1977. Wind loads on low-rise buildings: Final Report on Phases I and II – Parts 1 and 2: Text and Figures. BLWT-SS8, University of Western Ontario, London, Ontario, Canada.
- Davenport, A.G., Surry, D. and Stathopoulos, T. 1978. Wind loads on low-rise buildings: Final Report on Phase III. BLWT-SS4, University of Western Ontario, London, Ontario, Canada.
- Doudak, G. 2005. Field Determination and Modeling of Load Paths in Wood Light-Frame Structures. PhD Thesis, Department of Civil Engineering and Applied Mechanics, McGill University, Montreal, Quebec, Canada.
- Eaton, K.J., and Mayne, J.R. 1975. The measurement of wind pressures on two-storey houses at Aylesbury. *Journal of Wind Engineering and Industrial Aerodynamics*, **1**, 67-109.
- Levitan, M.L., Mehta, K.C., Chok, C.V., and Millsaps, D.L. 1990. An overview of Texas Tech's wind engineering field research laboratory. *Journal of Wind Engineering and Industrial Aerodynamics*, **36**(Part 2), 1037-1046.
- National Building Code of Canada - NBCC 2005. National Research Council of Canada, Ottawa.

- Ng, H.H.T., and Mehta, K.C. 1990. Pressure measuring system for wind-induced pressures on building surfaces. *Journal of Wind Engineering and Industrial Aerodynamics*, **36**(1-3), 351-360.
- Robertson, A.P., and Glass, A.G. 1988. The Silsoe structures building - its design, instrumentation and research facilities. AFRC Inst. Engng. Res., Silsoe, Div. Note DN 1482.
- Zisis, I., and Stathopoulos, T. 2009. Wind-induced cladding and structural loads on a low wooden building. *Journal of Structural Engineering, ASCE*, **135**(4), 437-447.

List of figure captions

Fig. 1. External dimensions of the experimental house.

Fig. 2. Location of foundation/roof load cells and pressure taps on the experimental house.

Fig. 3. Pressure tap location on the wind tunnel model and wind angles of attack tested in the wind tunnel experiments.

Fig. 4. Power law exponents of the three upstream terrain configurations used in the wind tunnel.

Fig. 5. Power law exponent variation with respect to direction.

Fig. 6. Turbulence intensity variation with respect to direction.

Fig. 7. Roughness length variation with respect to direction.

Fig. 8. Mean and peak pressure coefficient comparison (wall pressure tap NW,10).

Fig. 9. Mean and peak pressure coefficient comparison (roof pressure tap R,19).

Fig. 10. Pressure coefficient comparison between full-scale and respective wind tunnel results (full-scale record: May 14th, 2009).

Fig. 11. Pressure coefficient comparison between full-scale and respective wind tunnel results (full-scale record: June 1st, 2009).

Fig. 12. Test house and wall segment notations.

Fig. 13. Wall segment participation (SE, NW and SW, NE).

Fig. 14. Mean total uplift force coefficient comparison.

Fig. 15. Minimum and maximum peak total uplift force coefficient comparison.

Fig. 1. External dimensions of the experimental house.

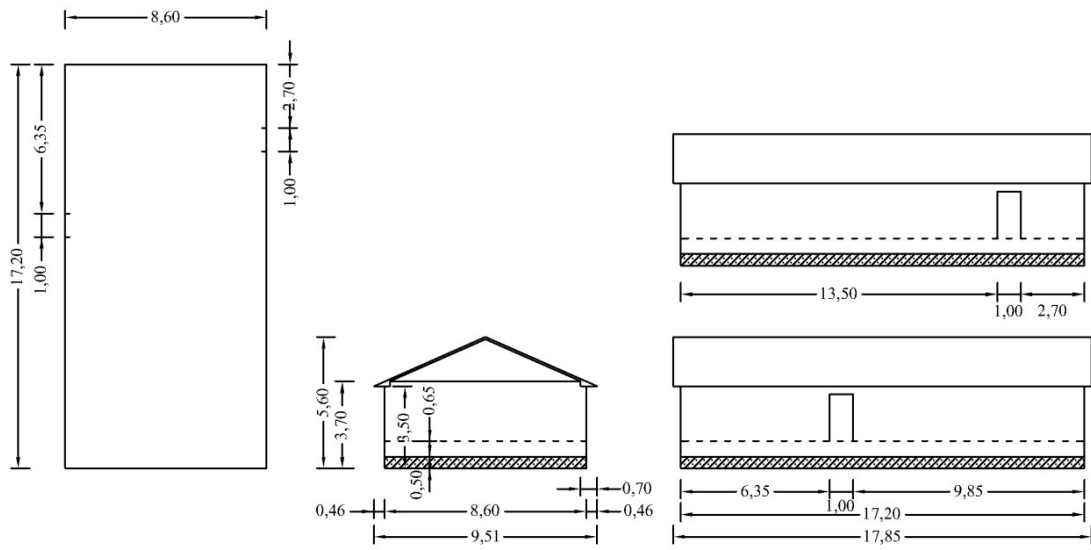


Fig. 2. Location of foundation/roof load cells and pressure taps on the experimental house.

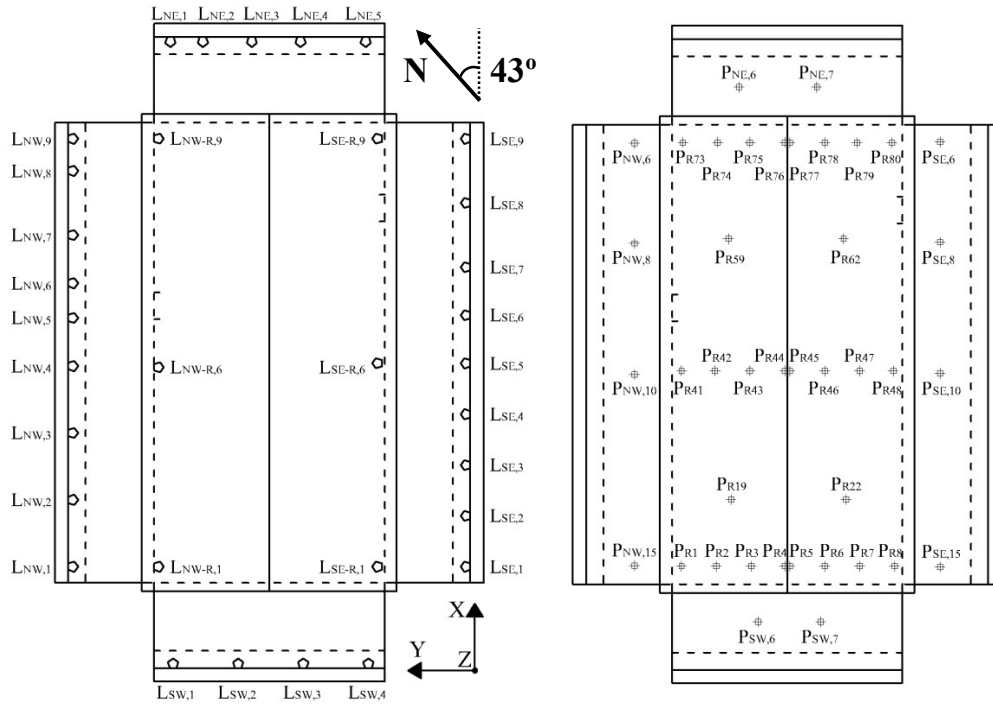


Fig. 3. Pressure tap location on the wind tunnel model and wind angles of attack tested in the wind tunnel experiments.

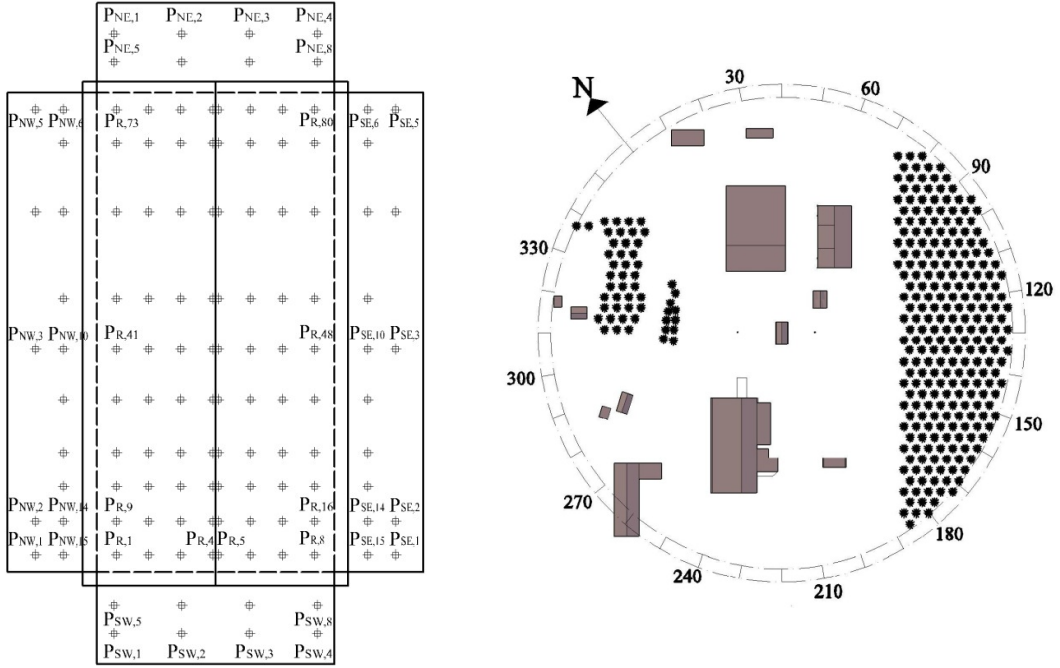


Fig. 4. Power law exponents of the three upstream terrain configurations used in the wind tunnel.

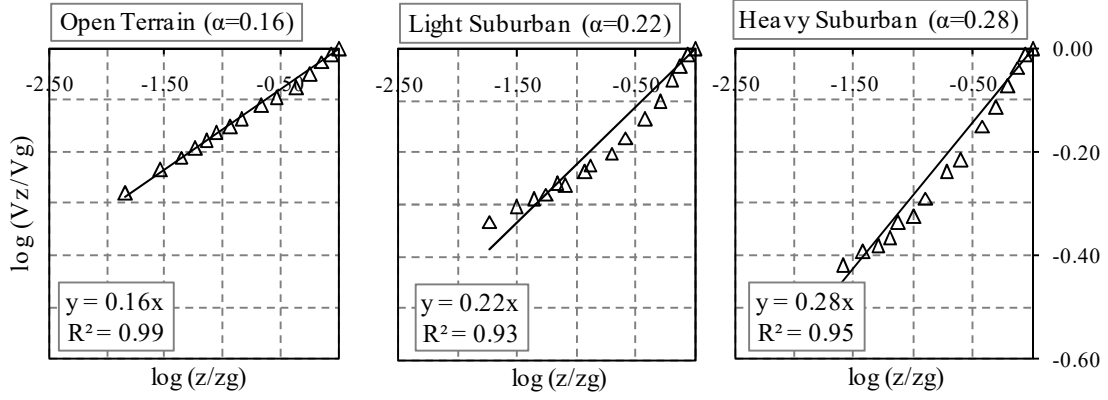


Fig. 5. Power law exponent variation with respect to direction.

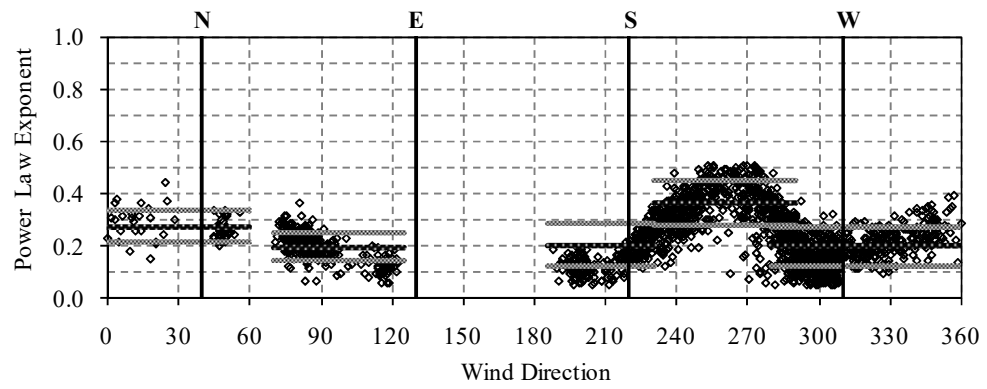


Fig. 6. Turbulence intensity variation with respect to direction.

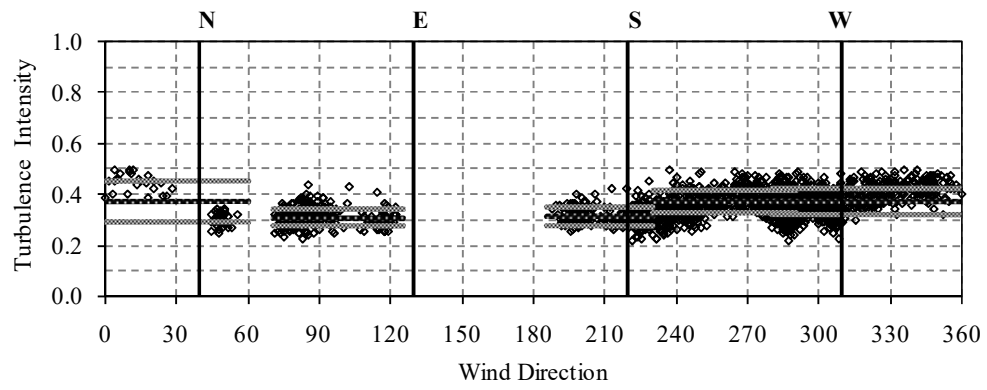


Fig. 7. Roughness length variation with respect to direction.

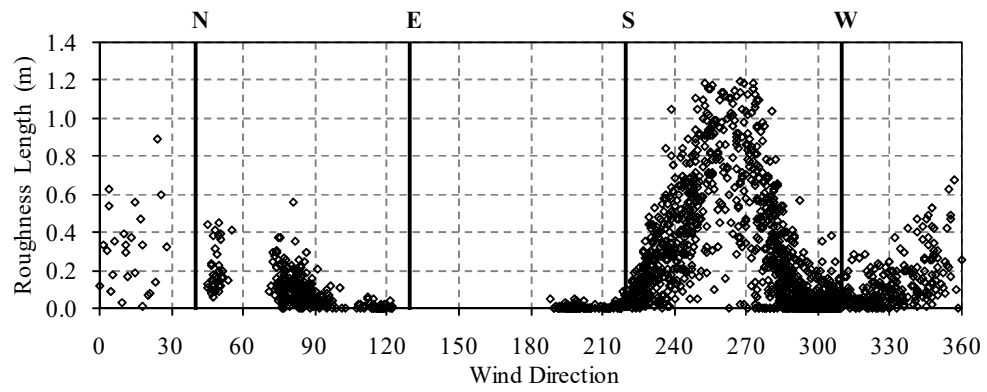


Fig. 8. Mean and peak pressure coefficient comparison (wall pressure tap NW,10).

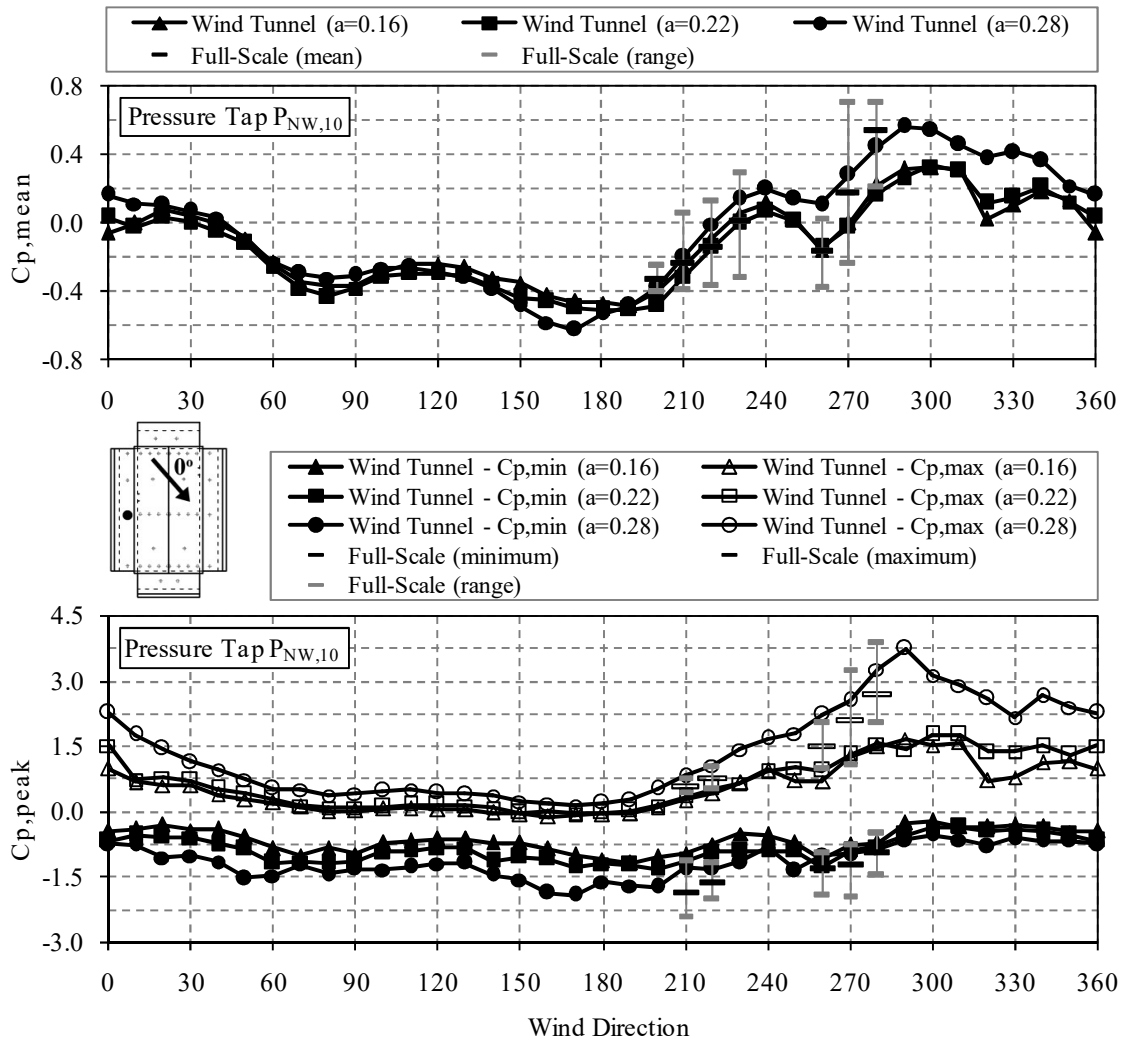


Fig. 9. Mean and peak pressure coefficient comparison (roof pressure tap R,19).

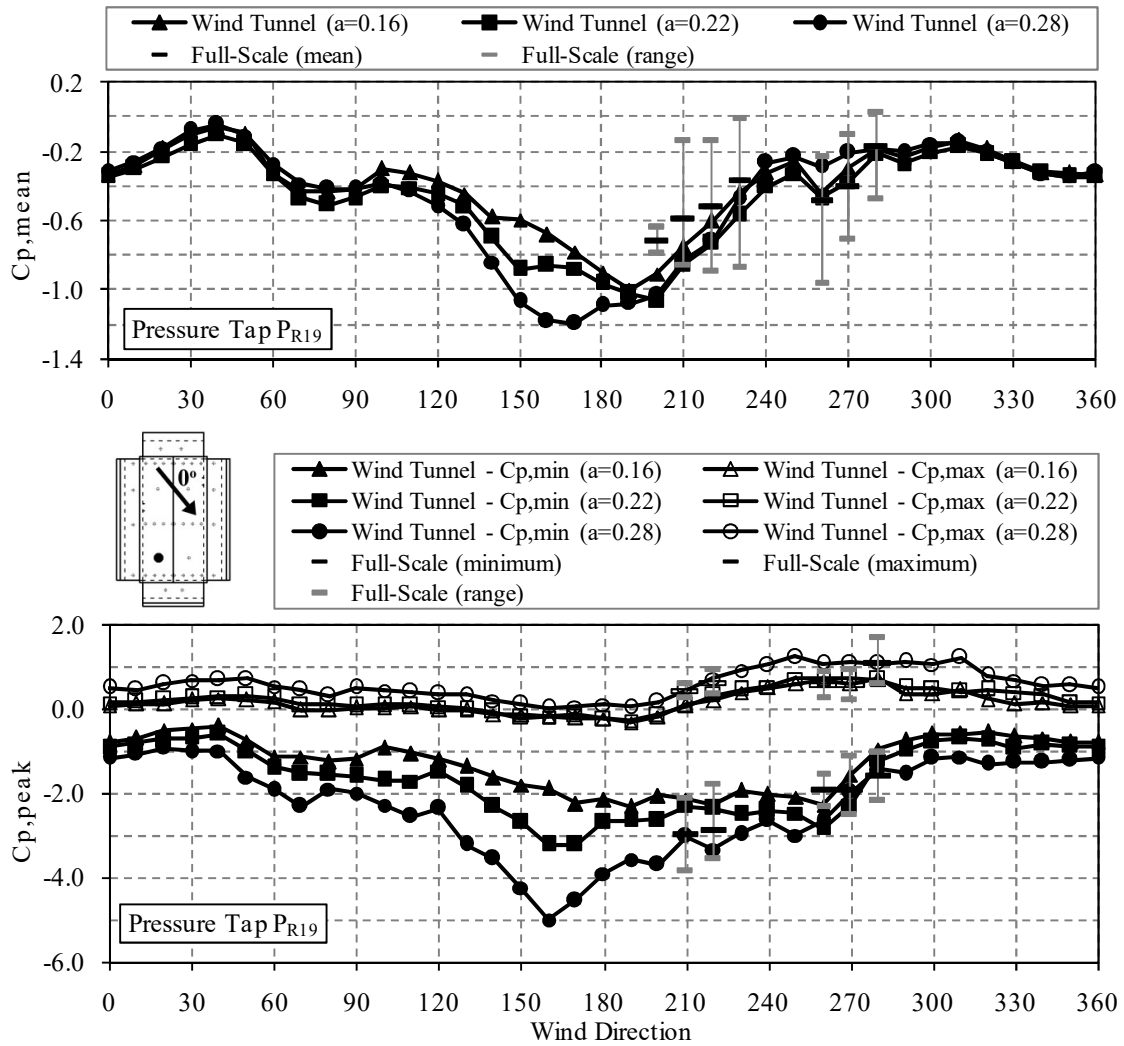


Fig. 10. Pressure coefficient comparison between full-scale and respective wind tunnel results (full-scale record: May 14th, 2009).

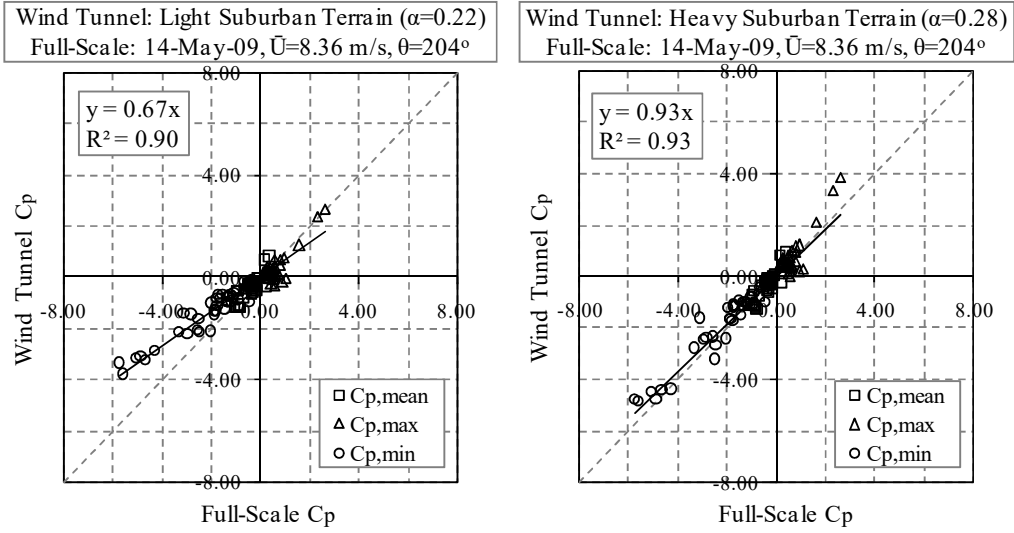


Fig. 11. Pressure coefficient comparison between full-scale and respective wind tunnel results (full-scale record: June 1st, 2009).

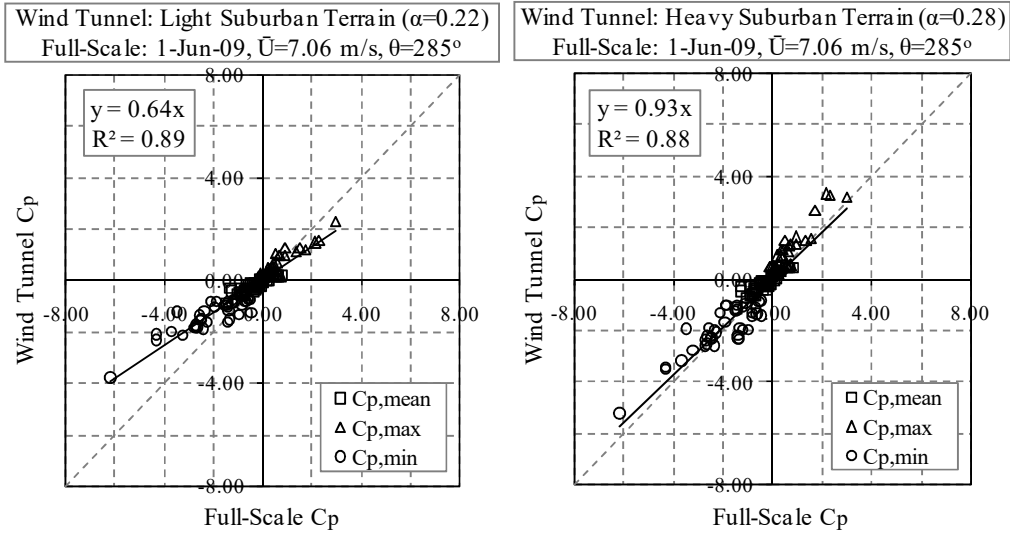


Fig. 12. Test house and wall segment notations.

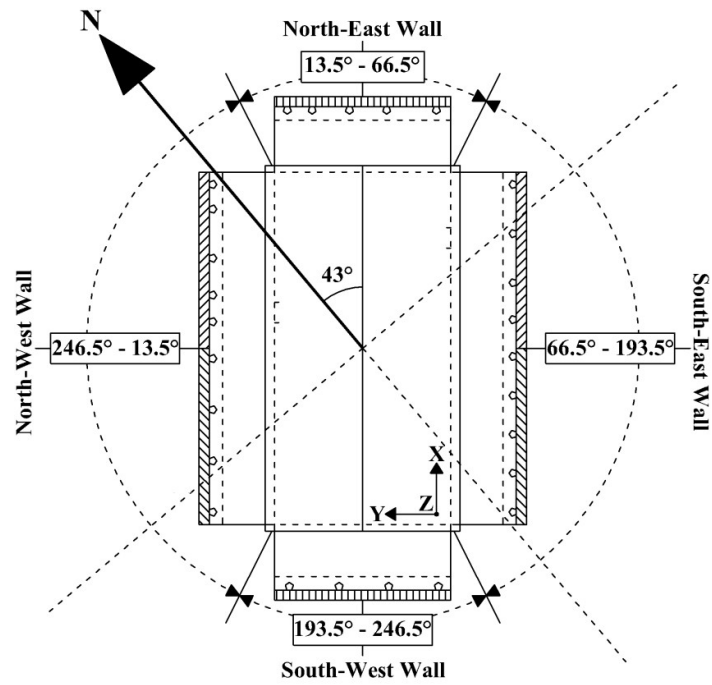


Fig. 13. Wall segment participation (SE, NW and SW, NE).

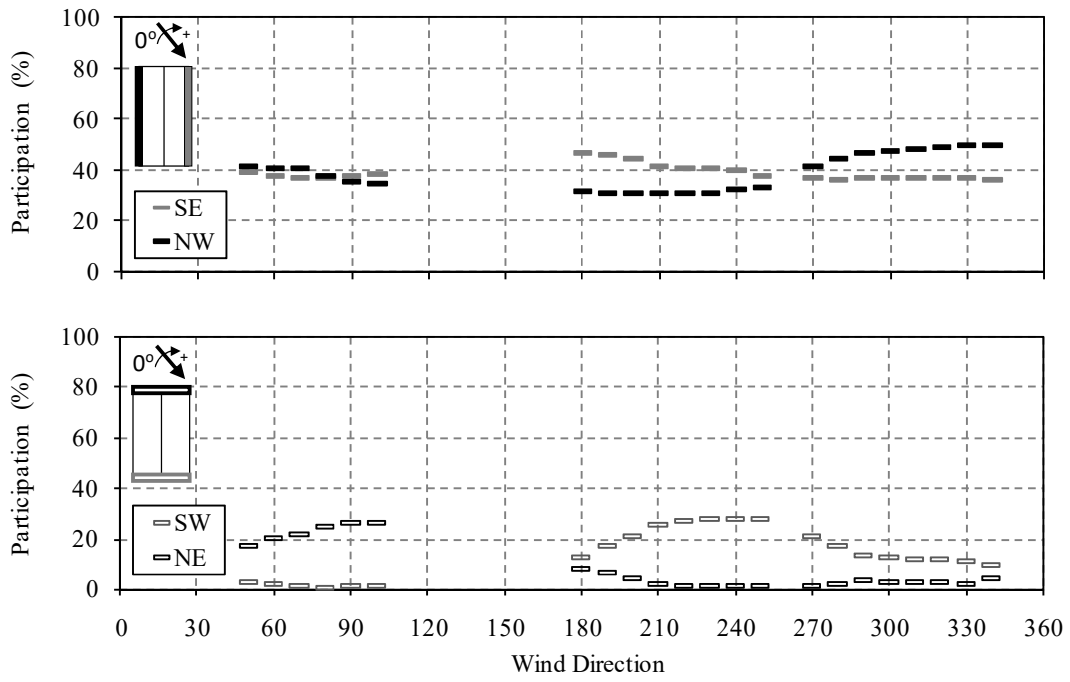


Fig. 14. Mean total uplift force coefficient comparison.

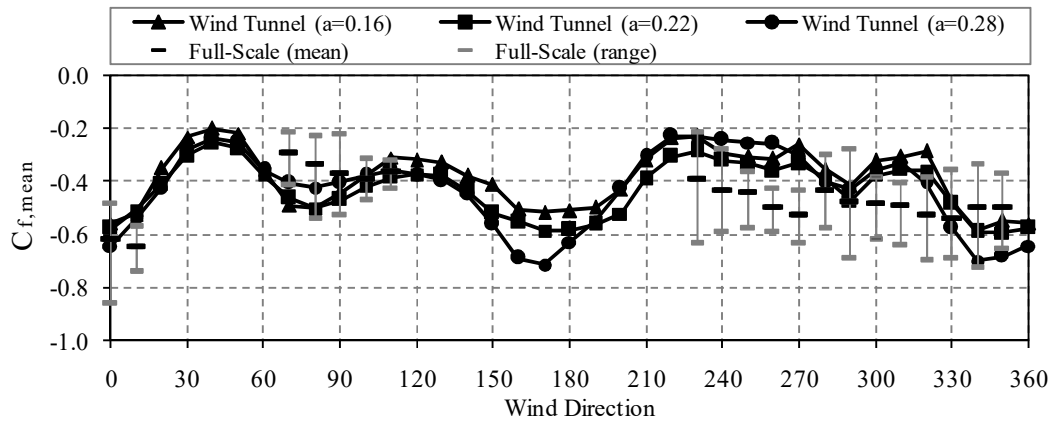


Fig. 15. Minimum and maximum peak total uplift force coefficient comparison.

